Nucleic Acids Research, 2020 **1**
doi: 10.1093/nar/gkaa211

PRMT7 regulates RNA-binding capacity and protein stability in *Leishmania* parasites

Tiago R. Ferreira [1], Adam A. Dowle [2], Ewan Parry [1], Eliza V. C. Alves-Ferreira [1], Karen Hogg [3], Foteini Kolokousi [1], Tony R. Larson [2], Michael J. Plevin [1], Angela K. Cruz [4] and Pegine B. Walrad [1,*]

[1]York Biomedical Research Institute, Department of Biology, University of York, York, UK, [2]Metabolomics and Proteomics Lab, Bioscience Technology Facility, Department of Biology, University of York, UK, [3]Imaging and Cytometry Lab, Bioscience Technology Facility, Department of Biology, University of York, UK. and [4]Cell and Molecular Biology Department, Ribeirão Preto Medical School, University of São Paulo, Ribeirão Preto, Brazil

Received August 12, 2019; Revised March 17, 2020; Editorial Decision March 19, 2020; Accepted April 16, 2020

ABSTRACT

RNA binding proteins (RBPs) are the primary gene regulators in kinetoplastids as transcriptional control is nearly absent, making *Leishmania* an exceptional model for investigating methylation of non-histone substrates. Arginine methylation is an evolutionarily conserved protein modification catalyzed by Protein aRginine Methyl Transferases (PRMTs). The chromatin modifier PRMT7 is the only Type III PRMT found in higher eukaryotes and a restricted number of unicellular eukaryotes. In *Leishmania major*, PRMT7 is a cytoplasmic protein implicit in pathogenesis with unknown substrates. Using comparative methyl-SILAC proteomics for the first time in protozoa, we identified 40 putative targets, including 17 RBPs hypomethylated upon PRMT7 knockout. PRMT7 can modify Alba3 and RBP16 *trans*-regulators (mammalian RPP25 and YBX2 homologs, respectively) as direct substrates *in vitro*. The absence of PRMT7 levels *in vivo* selectively reduces Alba3 mRNA-binding capacity to specific target transcripts and can impact the relative stability of RBP16 in the cytoplasm. RNA immunoprecipitation analyses demonstrate PRMT7-dependent methylation promotes Alba3 association with select target transcripts and thus indirectly stabilizes mRNA of a known virulence factor, δ-*amastin* surface antigen. These results highlight a novel role for PRMT7-mediated arginine methylation of RBP substrates, suggesting a regulatory pathway controlling gene expression and virulence in *Leishmania*. This work introduces *Leishmania* PRMTs as epigenetic regulators of mRNA metabolism with mechanistic insight into the functional manipulation of RBPs by methylation.

INTRODUCTION

Protein arginine methyltransferases (PRMTs) are widely distributed across eukaryotes in nine different classes of enzymes (PRMT1–9) (1). They catalyze arginine methylation in multiple cellular processes including histone modification, transcriptional control, RNA processing, protein localization and cell signaling (1–3). Histones and RNA-binding proteins (RBPs) have been characterized as PRMT substrates in multiple organisms (1,4).

PRMTs are classified as Type I, II or III according to the targeted nitrogen and number of methyl groups transferred (1) (Figure 1B). PRMT7 is a unique enzyme as it is the sole PRMT known to catalyze only monomethyl arginine (MMA; Type III PRMT), which may indicate a regulatory step that primes substrates prior to dimethylation (1,5). PRMT7 has been well described in mammalian cells as a histone methyl-transferase which modulates chromatin to repress gene promoters (6). Remarkably, the only unicellular eukaryotes known to carry a PRMT7 homolog are choanoflagellates and kinetoplastids, including *Leishmania*, where gene expression control is primarily post-transcriptional (4,7). The heightened regulatory role of RBPs in *Leishmania* can lend clear functional insight not obscured by complex networks of transcriptional regulation (8).

Leishmania spp. parasites are the causative agent of the leishmaniases, infectious diseases that contribute the ninth largest global disease burden, with 1 million new cases diagnosed annually (9). We have previously shown that *Leishmania major* PRMT7 expression regulates host pathology, is stage-regulated during development and is cytoplasmic-

*To whom correspondence should be addressed. Email: pegine.walrad@york.ac.uk
Present address: Tiago R. Ferreira, National Institute of Allergy and Infectious Diseases, National Institutes of Health, Bethesda, MD, USA.

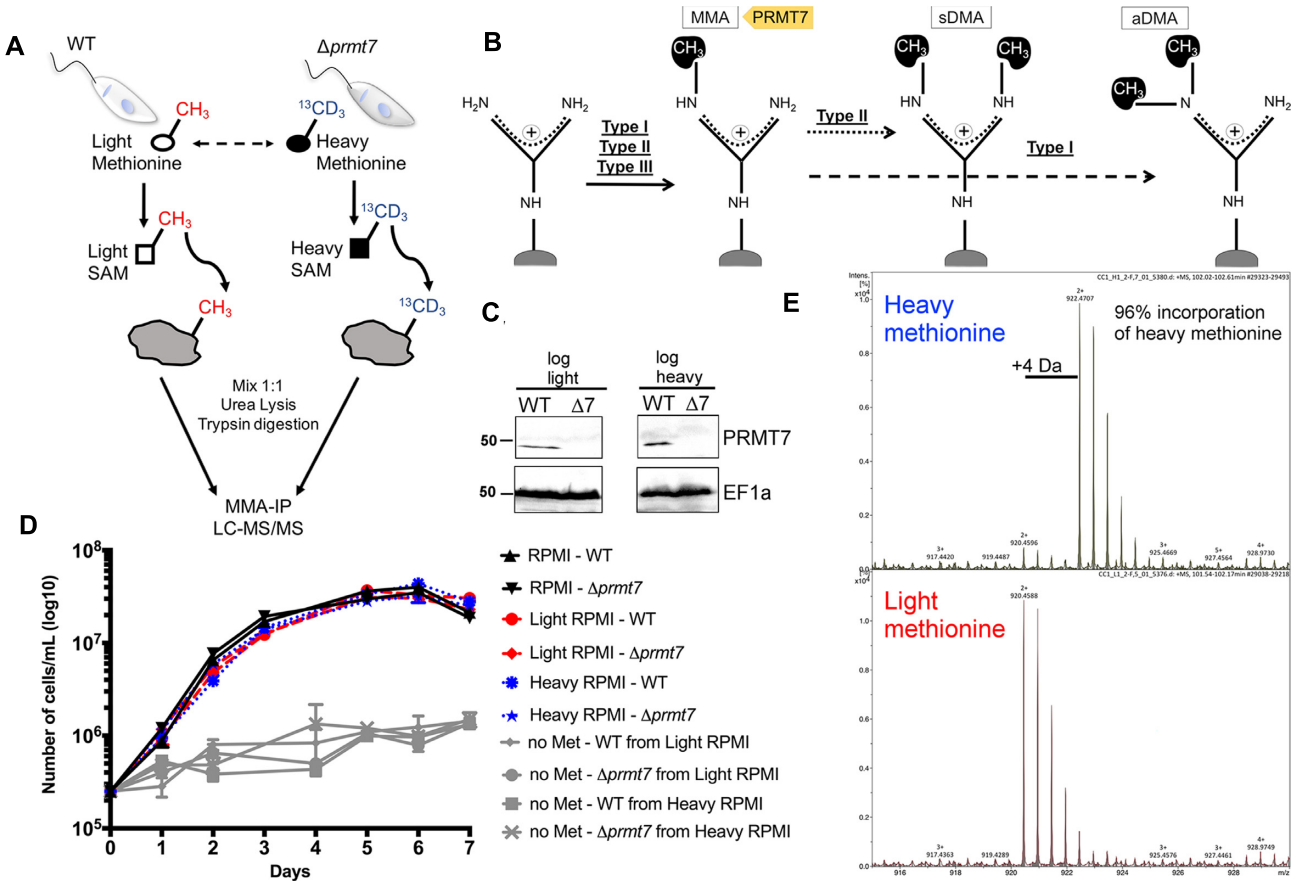

Figure 1. Heavy methyl SILAC is a feasible approach in *Leishmania major* promastigotes and does not significantly affect promastigote culture growth. (**A**) *L. major* wild-type (WT) and PRMT7 knockout (Δ*prmt7*) parasites were kept in SILAC media in the presence of light or heavy methionine (L-methionine-methyl-13C,d3) with label-swap replications. Tryptic peptides were submitted to anti-monomethyl arginine (20) immunoprecipitation and LC–MS/MS for identification and quantification of methyl peptides. (**B**) PRMT7 is the single Type III methyltransferase identified to date and thus catalyzes only MMA. Type II and Type I PRMTs catalyze, respectively, symmetric dimethylarginine (sDMA) and asymmetric dimethylarginine, in addition to MMA in a first step. (**C**) Expression of PRMT7 in logarithmic growth phase promastigotes was evaluated by immunoblotting for comparison between light and heavy SILAC media, which showed no significant difference. EF1a levels are shown for protein loading control. Blots are representative of a biological duplicate. (**D**) WT and Δ*prmt7* promastigotes growth curves were not significantly altered in different SILAC media (light or heavy RPMI). If methionine is not added to the culture media (no Met) parasite growth is not significant, which confirms the successful removal of methionine from the dialyzed fetal bovine serum. Data are plotted as mean ± standard error from three biological replicates. (**E**) MS spectra of a representative WT-derived peptide showing 96% incorporation of heavy methionine.

specific in contrast to the primarily-cytoplasmic, partially nuclear mammalian PRMT7 (5,10,11). Remarkably, the *Leishmania* PRMT7-directed regulatory pathway epigenetically controls parasite gene expression, and impacts host pathology four differentiation events and months after PRMT7 protein expression (10,12).

The impact of PRMT7 on the overall MMA-modified proteome is still unknown. To date, histones are the only mammalian PRMT7 targets validated *in vivo* (1,6,13). In contrast, *L. major* PRMT7 displays distinct localization, low sequence similarity and is nonessential. Combined with the negligible transcriptional control in *Leishmania* spp., all evidence suggests a divergent function between human and *Leishmania* PRMT7 enzyme (10). A recent large-scale study compared the distribution of arginine residues across eukaryotes and found that unicellular organisms that carry a PRMT7 homolog (including *Monosiga brevicolis* and *Leishmania infantum*) have a higher ratio of predicted methylarginine/unmodified arginine than others (*Plasmodium falciparum* and *Dictyostelium discoideum*) (14). Indeed both *L. major* and *Trypanosoma brucei* PRMT7s are distinct enough from mammalian orthologs that the regulatory pathways they drive may present anti-parasitic drug targets or an opportunity to repurpose existing drugs (2,4,10). We previously linked PRMT7 levels to *L. major* parasite virulence and leishmaniasis pathogenesis (10).

Here, we present the first comprehensive investigation of the molecular impact of modulating PRMT7 levels and the first quantified identification of a *Leishmania* arginine monomethyl proteome. Using methyl-SILAC proteomics, we identified 247 arginine monomethylated proteins, including 62 RNA-binding proteins (RBPs); 17 of which are hypomethylated upon PRMT7 knockout. RBPs are the primary genetic regulators in *Leishmania* species as genes are constitutively transcribed (8). We further validate PRMT7 methylation targets both *in vitro* and *in vivo* and reveal arginine methylation as an important post-translational regulator of RBP function with differential impact upon indi-

vidual *trans*-regulators. PRMT7-dependent monomethylation promotes cytoplasmic RBP16 protein stability as well as controls the highly selective mRNA binding capacity of Alba3; stabilizing *δ-amastin* surface antigen mRNA levels but not impacting association or stability of *nmt* transcript target. The near-absence of transcriptional control in *Leishmania* amplifies the regulatory role of *trans*-regulators and renders it an excellent system to investigate the impact of PTMs on RBP function (7). This study introduces *Leishmania* PRMTs as epigenetic regulators of downstream parasite virulence via modified RBP protein expression, selective RNA binding capacity and subsequent mRNA metabolism.

MATERIALS AND METHODS

Leishmania major cultures and transfection

Leishmania major promastigotes strain CC1 (MHOM/IR/83/LT252) were cultured at 26°C in M199 medium supplemented with 40 mM HEPES, 10% FBS, 100 U penicillin/ml, 100 μg/ml, 100 μM adenine, 0.0005% Hemin. In the phlebotomine vector, *L. major* parasites differentiate from the proliferative non-infective procyclic promastigotes to the non-dividing human-infective metacyclic promastigotes, a metacyclogenesis process that is mimicked in culture (15). Procyclics and metacyclics are enriched in axenic culture, respectively, at log and stationary growth phases. Inside mammalian phagocytic cells (primarily macrophages) metacyclic promastigotes differentiate into non-motile amastigotes.

PRMT7 knockout parasites (Δ*prmt7*) were previously generated as described (10). Plasmid and PCR oligos used in this study are shown in Supplementary Figure S2 and Supplementary Table S3, respectively. The coding sequence (CDS) and 500 bp 5′ flanking region (FLR) of RNA-binding proteins Torus (*LmjF.36.0740*), DDX3 (*LmjF.32.0400*), RBP16 (*LmjF.28.0825*) and Alba3 (*LmjF.34.2580*) were PCR amplified. The cloning strategy involved using four different *Sfi*I enzyme sites to allow a single-step four-way ligation: SfiA (GGCCACCTAG GCC), SfiB reverse (GGCCACGCAGGCC), SfiC (GGCC GCTGGGGCC) and SfiD reverse (GGCCTGACTGGC C) (16). PCR products were purified using NucleoSpin Gel and PCR Clean-up (Macherey-Nagel), cloned into pGEM®Teasy vector (Promega), SfiI digested and ligated into plasmid pFLAG_HA-RBP (Supplementary Figure S2A). Positive clones were confirmed by diagnostic restriction and sequencing, *Pme*I–*Pac*I digested overnight and purified DNA was transfected into *L. major* WT and Δ*prmt7* using Amaxa Nucleofector IIb (Lonza). Transfectants were selected on 1% agar M199 plates with 10 μg/ml G418 and PCR-validated using 5′FLR and 3′FLR primers (Supplementary Figure S2B and C).

Alba3 hypomethylated mutants were generated by replacing arginine residues (RG/RGG motifs) in the C-terminus to either tryptophan (WGG) or lysine (R192K or KGG) and inserting each construct into pFLAG_HA-Alba3. For the latter, *alba3* sequence was modified by Q5® Site-Directed Mutagenesis (New England Biolabs) using oligos shown in Supplementary Table S3 to either replace a single arginine detected in the MMA methyl-SILAC analysis ($Alba3^{R192K}$) or all the eleven arginine residues in RGG motifs present in its C-terminal tail ($Alba3^{KGG}$). The $Alba3^{WGG}$ mutant sequence was obtained as a custom synthetic gene (GenScript), in which each of the eleven arginine residues were mutated. Final constructs were transfected into both WT and Δ*prmt7 L. major* cell lines.

Parasite labeling by SILAC

Heavy methyl-SILAC has been shown to provide high confidence methyl peptide matches, and it is considered the optimal method for identifying protein methylation in large-scale proteomics (17). Parasites were cultured for 10 passages in SILAC-RPMI media (RPMI lacking Methionine (Dundee Cell Products), 10% 3.5 kDa-dialyzed serum, 20 mM HEPES pH 7.4, 100 μM adenine, 20 mM L-glutamine, 100 U/ml penicillin, 100 μg/ml streptomycin, 1 μM biopterin, 0.0005% hemin) supplemented with either L-methionine or L-methionine-methyl-$^{13}CD_3$ (Sigma-Aldrich), for 10 passages corresponding to approximately 100 parasite divisions. L-Methionine is converted into *S*-adenosylmethionine (18), the main biological methyl donor for transmethylation reactions, which allows direct labeling of methylated substrates (3). Next, J774.2 macrophages kept in SILAC-RPMI media for 4 passages were infected with late-stationary phase promastigotes at a 10:1 ratio to obtain recently differentiated promastigotes, as prolonged axenic promastigote culturing can alter virulence-related features (19). Three hours post-infection, plates were washed in incomplete RPMI and kept for 48 h under the same conditions. Amastigotes were purified and differentiated into procyclic promastigotes in SILAC-RPMI at 26°C and cultured for three passages.

Parasite protein extraction and enrichment of monomethylated arginine peptides

Procyclic promastigote (10^9 parasites) were pelleted at 2000 g for 10 min, washed in PBS and lysed (20 mM HEPES pH 8.0, 9 M urea, 1 mM sodium orthovanadate, 2.5 mM sodium pyrophosphate, 1 mM β-glycerophosphate) via three rounds of sonication at 15 W for 15 s at room temperature (RT) to avoid urea precipitation with 1 min intervals on ice. Lysates were cleared at 20 000 g, 20 min, 15°C and supernatants were collected.

Sample preparation and enrichment of monomethyl arginine peptides (20) were conducted using PTMScan[mme-RG] kit (Cell Signaling Technology) according to manufacturer's protocols with the following modifications; proteins were reduced in 4.5 μM DTT at 55°C for 30 min, cooled on ice and alkylated in 2 mg/ml iodoacetamide at RT for 15 min. Lysates were diluted 3-fold in 20 mM HEPES pH 8.0 and digested overnight in 10 μg/ml trypsin-TPCK (Sigma-Aldrich) and 10 μM HCl, at RT under agitation. Digestion was confirmed by SDS-PAGE and Coomassie Blue R staining. Digests were acidified with trifluoroacetic acid (21) to a final concentration of 0.1% and a pH strip was used to confirm pH <3. Precipitate was formed at RT for 15 min. Peptides were purified using a Sep-Pak C_{18} column (Waters) connected to a 10 cc reservoir, pre-wet in 5 ml 100% acetonitrile and washed sequentially in 1, 3 and 6 ml 0.1% TFA. Acidified peptide solution was cleared at 1800 g for

15 min at RT and cleared supernatant was loaded onto the C_{18} column using a 10 cc plunger. The column was washed sequentially in 1, 5 and 6 ml 0.1% TFA and then in 2 ml 5% acetonitrile, 0.1% TFA. Peptides were collected by three elutions in 2 ml 40% acetronitrile, 0.1% TFA and dried in a Speed-Vac concentrator for ∼3 h.

Dry peptide pellets were dissolved in 1.4 ml Immunoaffinity Purification (IAP) buffer (CST) and pH ∼7.0 was confirmed on a pH strip. All subsequent steps were performed on ice or at 4°C. Peptide solution was cleared at 10 000 g for 5 min and supernatant was transferred to a fresh tube. Anti-MMA agarose beads from the PTMScan kit (CST) were washed four times at 2000 g for 1 min, in 1 ml PBS (8 mM Na_2HPO_4; 1.5 mM NaH_2PO_4; 2.7 mM KCl; 137 mM NaCl; pH 7.0) and resuspended in 40 μl PBS. Peptide solution was mixed with the anti-MMA beads and incubated for 2 h under rotation. Peptide-beads slurry was centrifuged at 2000 g for 1 min and unbound peptides were collected and kept at –80°C. Beads were washed twice in 1 ml IAP buffer and three times in HPLC-grade water; inverting the tube five times and centrifuged at 2000 g for 1 min. MMA peptides were collected by two elutions in 55 μl of 0.15% TFA at RT for 10 min, mixing every 2 min, and centrifuged at 2000 g for 1 min.

Eluted monomethyl peptides were concentrated and purified using a Ziptip (Merck-Millipore). The Ziptip was first equilibrated in 50 μl of 50% acetronitrile, 0.1% TFA and twice in 50 μl of 0.1% TFA. IP eluent was loaded by passing through the Ziptip 10 times. Tips were washed twice in 0.1% TFA and peptides were eluted in 10 μl 40% acetonitrile, 0.1% TFA at least 10 times. Ziptip eluent was precipitated in a Speed-Vac and MMA peptides were resuspended in 10 μl of 0.1% TFA.

Mass spectrometry data acquisition and analysis

Samples were loaded onto an UltiMate 3000 RSLCnano HPLC system (Thermo) equipped with a PepMap 100 Å C_{18}, 5 μm trap column (300 μm × 5 mm, Thermo) and a PepMap, 2 μm, 100 Å, C_{18} EasyNano nanocapillary column (75 μm × 150 mm, Thermo). The trap wash solvent was 0.05% (v:v) aqueous trifluoroacetic acid and the trapping flow rate was 15 μl/min. The trap was washed for 3 min before switching flow to the capillary column. Separation used gradient elution of two solvents: solvent A, aqueous 1% (v:v) formic acid; solvent B, aqueous 80% (v:v) acetonitrile containing 1% (v:v) formic acid. The flow rate for the capillary column was 300 nl/min and the column temperature was 40°C. The linear multi-step gradient profile was: 3–10% B over 8 min, 10–35% B over 125 min, 35–65% B over 50 min, 65–99% B over 7 min and then proceeded to wash with 99% solvent B for 4 min. The column was returned to initial conditions and re-equilibrated for 15 min before subsequent injections.

The nanoLC system was interfaced with an Orbitrap Fusion hybrid mass spectrometer (Thermo) with an EasyNano ionization source (Thermo). Positive ESI-MS and MS^2 spectra were acquired using Xcalibur software (version 4.0, Thermo). Instrument source settings were: ion spray voltage, 1900 V; sweep gas, 0 Arb; ion transfer tube temperature; 275°C. MS^1 spectra were acquired in the Orbitrap with: 120 000 resolution, scan range: m/z 375–1500; AGC target, $4e^5$; max fill time, 100 ms. Data dependent acquisition was performed in top speed mode using a 1 s cycle, selecting the most intense precursors with charge states 2–5. Dynamic exclusion was performed for 50 s post precursor selection and a minimum threshold for fragmentation was set at $3e^4$. MS^2 spectra were acquired in the linear ion trap with: scan rate, rapid; quadrupole isolation, 1.6 m/z; activation type, HCD; activation energy: 32%; AGC target, $5e^3$; first mass, 110 m/z; max fill time, 100 ms. Acquisitions were arranged by Xcalibur to inject ions for all available parallelizable time.

Peptide identification

Protein identification was performed using Sequest HT and Mascot. Thermo .raw files were submitted to Sequest HT database searching using Proteome Discoverer (version 2.1, Thermo). Peak lists were extracted following .raw to .mgf format conversion using MSconvert (version 3.0.9967, ProteoWizard) before submitting via Mascot Daemon (version 2.5.1, Matrix Science Ltd) to a local-running copy of the Mascot program (version 2.5.1, Matrix Science Ltd). Database searching was performed against the TriTrypDB (version 8.1) (18) *L. major* Friedlin genome (8400 sequences). Search criteria specified: Enzyme, trypsin; Fixed modifications, carbamidomethyl (C); variable modifications, oxidation (M), phospho (ST), methyl (R), methyl (K), methyl: 2H(7)13C(1) (R), Label: 13C(1)2H(7) (M), Label: 13C(1)2H(7) + oxidation (M); peptide tolerance, 5 ppm; MS/MS tolerance, 0.5 Da; maximum missed cleavages, 3; instrument, ESI-TRAP. Scaffold PTM (version 3.0.0, Proteome Software) was used to calculate methylation site localization probabilities for Mascot derived peptide identifications using the algorithm as described (22). Briefly, MS^2 spectra identified as originating from methylated peptides were re-analyzed to calculate Ascore values and site localization probabilities to assess the level of confidence in each PTM positional assignment. Scaffold PTM then combined localization probabilities for all peptides containing each identified PTM site to obtain the best estimate probability that a PTM is present at that particular site.

Relative quantification of methylated peptides

A list of unique, methylated peptides was compiled from Sequest and Mascot identifications across all samples post-filtering to require posterior error probabilities <0.05. The list was used to calculate theoretical m/z values for the light and heavy analogues of all identified methylated peptides. Observed retention times from search results were associated with theoretical m/z pairs and appended to the mass list to create an extracted ion chromatogram (XIC) target list. Where methylated peptides were identified multiple times the median retention time was used. Thermo .raw files were converted to .mzML using Bioconductor (version 3.5) in R (version 3.3.1) before processing using the xcms package (23). XICs were extracted for all theoretical light and heavy m/z pairs across retention time aligned samples within 60 s windows, and peak areas extracted us-

ing the centWave algorithm (24). Light and heavy peak areas were normalized to relative % (light/heavy) and the reciprocal % (heavy/light) calculated for replicates originating from switched light to heavy metabolic labeling. Significance testing for quantitative differences between normalized light and heavy peak areas was performed using Student's t-test (two-tailed, heteroscedastic). Calculated *P*-values were multiple-test corrected using the Hochberg and Benjamini FDR estimation. Accepted differences were required to have corrected *P*-values <0.05, be derived from XIC peak areas in >2 samples and be observed consistently in at least one replicate upon light to heavy metabolic label switching.

Bioinformatic analyses of PRMT7 MMA RNA binding protein targets

Amino acid sequences of 18 PRMT7 RBP targets were downloaded from TriTrypDB.org (18) and subjected to a set of bioinformatic tools to predict the type and location of constituent domains. Initial Pfam (25) domain annotations were obtained using BLASTP (23) and RefSeq and PDB sequence databases. Predictions of secondary structure and intrinsic disorder were performed using PSIPRED (26) and DISOPRED (27), respectively. Additional structural predictions were conducted using Phyre2 in standard mode (28). The results of these analyses were combined to inform manual predictions of likely domain boundaries and to annotate domain type and function. Extended regions of predicted secondary structure and low disorder that lacked a clear functional annotation were assigned as domains of unknown function (DUF).

In vitro methylation assay by PRMT7

Recombinant proteins were expressed in *Escherichia coli* BL21(DE3)pLys using pET28a+ (Novagen) and purified using Ni-Sepharose affinity medium (GE Healthcare). Purified and dialyzed proteins were analyzed on SDS-PAGE and had their identity verified by mass spectrometry. PRMT7 wild-type and mutants were incubated with putative substrates in PBS with 2 μCi of *S*-adenosyl-[methyl-3H]methionine ($^{[3H]}$AdoMet) (55–85 Ci/mmol, PerkinElmer) for 18 h at 26°C. Reactions were then halted by the addition of 2× SDS sample buffer (125 mM Tris–Cl pH 6.8, 20% glycerol, 2% SDS, 0.7 M β-mercaptoethanol and 0.01% bromophenol blue) at 95°C for 5 min. Human histone H4 was used as a positive control for PRMT7 activity (1 μg per reaction; New England Biolabs). Reactions were loaded and run on 12.5% SDS-PAGE and gels were dried on Whatman paper for 2 h at 80°C on a gradient drying cycle. The dried gel was exposed to Hyperfilm (GE Healthcare) for 3–14 days at –70°C. Gels were also stained with Coomassie R for loading control. Gels and films were scanned on an ImageScanner III (GE Healthcare) for posterior analysis using GIMP (GNU Image Manipulation Program).

Immunoblotting

Mid-log or stationary promastigotes were pelleted at 2000 g for 10 min, washed in PBS, lysed in 2X SDS sample buffer, boiled 5 min and loaded (10^7 cells per lane) on 12.5% SDS-PAGE gels. Proteins were transferred to PVDF membranes at 20 V for 1 h using a Novex Semi-Dry blotter (Thermo). Blots were blocked in 5% milk TBS-T (20 mM Tris, 150 mM NaCl, pH 7.4, 0.05% Tween) for 1 h at RT, or 5% BSA TBS-T for anti-PRMT7 blots. Primary antibodies were diluted in 1% milk or BSA TBS-T: mouse anti-HA [1:20 000] (Thermo); rabbit anti-MMA [1:3000] (MultiMab, CST); chicken anti-*Lmj*PRMT7 [1:1000] (10), rabbit anti-*Tb*RBP16 [1:1000] (29) and mouse anti-EF1a [1:200 000] (clone CBP-KK1, Merck-Millipore) for 18 h at 4°C. Blots were briefly washed five times in TBS-T and incubated in secondary antibodies for 1 h. Membranes were washed and incubated in ECL Prime (GE Healthcare) detection solutions for 5 min prior to ECL Hyperfilm exposure (GE Healthcare).

Immunofluorescence

Procyclic or metacyclic promastigote cells were incubated in culture with 200 nM of MitoTracker™ Green FM (Molecular Probe) for 30 min at 26°C, harvest and antibody stained as described (30) using mouse anti-HA [1:500] (Sigma) or rabbit anti-*Tb*RBP16 [1:500] (29) and Alexa secondary antibodies [1:10 000]. Images were acquired on a Zeiss LSM 710 confocal microscope and images were processed using PerkinElmer Volocity software.

RNA immunoprecipitation and qRT-PCR

HA-Alba3 was immunoprecipitated from *in vivo* UV-crosslinked log-phase promastigotes with anti-HA magnetic beads (Thermo) as described (8,30). Crosslinking was performed with UVC using the LT40 'Minitron' system (UV03 Ltd) (21) for 120 s at 1.6 mJ/cm^2, which is less stressful to parasites and damaging to mRNA (8). Total RNA was extracted from WT and Δ*prmt7* input samples using Direct-zol RNA Miniprep (Zymo Research). cDNA was synthesized from 2 μg of total RNA or 100–400 ng of RIP RNA using the SuperScript IV Reverse Transcriptase (Invitrogen). Absolute quantification curves were performed for each oligonucleotide pair using serial dilutions of cDNA. Relative quantification (–ΔΔCt) was performed using the Fast SYBR Green Master Mix and Quantstudio 3 PCR System (Thermo Fisher) as described (8). RNA levels were normalized to the 18S rRNA and glycosomal glyceraldehyde 3-phosphate dehydrogenase (GAPDHg, *LmjF.30.2980*). GeneIDs of the mRNAs are: *NIMA-related kinase* (*LmjF.35.5190*), *nmt* (*LmjF.32.0080*), δ-*amastin* (*LmjF.34.0500*) and *p1/s1 nuclease* (*LmjF.30.1510*). Primers are listed in Supplementary Table S3.

Protein and mRNA decay

For protein stability evaluation, promastigotes at day 2 (log phase; non human-infective promastigote) or day 6 (stationary phase; human-infective promastigote) post-inoculum were incubated in 200 μg/ml cycloheximide at 26°C and harvested at time-points up to 24 h for western blotting as above. Membranes were stained post-transfer

in Ponceau for loading controls. Densitometry analysis was performed using ImageJ software (31).

For transcript stability analysis, log phase promastigotes were incubated up to 4 h in 5 μg/ml actinomycin D (Sigma) to inhibit *de novo* transcription (32). Cells (2×10^7) were harvested at specific time points and lysed in Trizol reagent (Invitrogen). Total RNA was extracted using Direct-zol RNA Miniprep (Zymo Research). RNA levels were quantified by qRT-PCR as above, normalized to 18S rRNA. Protein and mRNA half-life was calculated using Prism software (GraphPad) by a one-phase or two-phase decay exponential curve robust fit (according to the observed decay profile) with a Plateau constraint of 0.

RESULTS

RNA-binding proteins are the primary targets of arginine monomethylation in *L. major*

To evaluate the impact of PRMT7 loss upon the arginine monomethyl proteome of *L. major*, wild-type (WT) and Δ*prmt7* parasites were labeled with either L-methionine (33) or L-methionine-methyl-$^{13}CD_3$ (heavy) and submitted for methyl-SILAC proteomic analysis (Figure 1A). Expression of PRMT7 was similar between light and heavy methyl-labeled parasites (Figure 1C) and no significant growth difference was observed between WT and *Δprmt7* cells, light or heavy (Figure 1D). Heavy methionine incorporation of >95% was confirmed by LC–MS (Figure 1E), which is sufficient and essential for SILAC analyses (34).

Comprehensive peptide quantification by methyl-SILAC revealed 40 proteins hypomethylated in Δ*prmt7* cells (WT/Δ*prmt7* methyl peptide ratio >1.5) from the 247 MMA-containing proteins identified (≥2 peptides and detection in label-swap repetition; Figure 2A and B; Supplementary Table S1). In total, these proteins are represented by 387 unique MMA peptides identified. Mass spectrometry analysis of unfractionated peptides (input) did not show significant differential expression of total methylated proteins between wild-type and *Δprmt7* samples.

Molecular Function Gene Ontology (GO) Term analysis reveals that nucleic acid binding and RNA-binding functions are significantly enriched in the global MMA proteome and more prominently in the *Δprmt7* hypomethylated proteins (Figure 2C and D). Among 62 RNA-binding proteins (Supplementary Table S2), we found 24 differentially methylated in *Δprmt7* cells, of which 17 are hypomethylated and represent putative substrates of PRMT7 activity (Supplementary Table S2). Analysis of the peptide sequences surrounding the methylated arginines using WebLogo 3 (35) demonstrates differential residue selection between the hypomethylated arginines versus total MMA proteome in *Δprmt7* cells. The global MMA data do not present a significant motif consensus, with 10–20% probability for glycines to surround the methylarginine (Figure 2C). However, there is a strong selection evident for RG/RGG (or GR/GGR) motifs in the hypomethylated PRMT7 substrate peptides (Figure 2D), revealing a candidate target motif for the PRMT7 enzyme. Of interest, MMA sites in isolated hypomethylated RBPs reside outside conserved Interpro/Pfam domains (Figure 3), suggesting RBP–RNA interactions might not be directly obstructed.

Validating RBP substrates of PRMT7 methylation

From the list of proteins hypomethylated in Δ*prmt7*, we selected Alba3 (Alba20) (10,36,37) and RBP16 for further investigation (Figure 2A). Alba3 is a RPP25-like protein (ribonuclease P subunit p25-like) involved in the stabilization of the δ-*amastin* virulence factor mRNA upregulated in amastigotes (37). RBP16 is a Y-box binding protein (YBX2-like) important for trypanosomatid mitochondrial mRNA editing and stabilization (38). We previously identified these two RBPs as candidate targets of PRMT7 methylation (10). To determine whether these RBPs are direct targets of PRMT7 methylation, purified recombinant 6xHis-tagged PRMT7 (His-PRMT7) and putative substrates His-Alba3 and His-RBP16 were tested for activity *in vitro*. We first confirmed His-PRMT7 activity is detectable *in vitro* using a commercially available human Histone H4 (H4), a canonical target of mammalian PRMTs (Figure 4A) versus a protein containing 12 arginines but not an identified target, prostaglandin f2-alpha synthase (PGF2S) (39). PGF2S is not methylated by PRMT7 *in vitro* (Figure 4A–C).

Next, we examined His-PRMT7 methylation of recombinant His-RBP16 and His-Alba3, as well as a mutant protein devoid of the RGG-rich C-terminal tail (His-Alba3$^{\Delta RGG}$, Figure 4B). His-PRMT7 methylates His-Alba^{WT} and His-RBP16^{WT} *in vitro* in a concentration-dependent manner but not His-Alba3$^{\Delta RGG}$ (Figure 4C). This indicates that recombinant PRMT7 is sufficient to monomethylate both RBP targets directly and that PRMT7-catalyzed methylation requires the C-terminal RGG motifs of Alba3, despite 18 additional non-RGG arginine residues still present in His-Alba3$^{\Delta RGG}$.

Building upon these observations, we generated two catalytically-inactive PRMT7 mutants to confirm conservation of the catalytic site in *Leishmania* and the specificity of the observed methylation signal (Figure 4B, D). In other eukaryotes, key glutamate (E) residues in the double E loop of the SAM-binding domain have been replaced to generate inactive PRMT mutants (40,41). Analysis of the double E loop sequence of PRMTs in *L. major* showed conservation of residues E202 and E211 (Supplementary Figure S1). The first glutamate residue in this domain (E202) was mutated to either a glutamine or lysine accordingly (Figure 4B). In contrast to His-PRMT7^{WT}, recombinant His-PRMT7^{E202Q} and His-PRMT7^{E202K} do not methylate His-Alba3 or His-RBP16 *in vitro* (Figure 4D). These results confirm the catalytic domain and the double E loop are essential for PRMT7-dependent monomethylation of RBP targets *in vitro*.

Loss of PRMT7 impacts RBP expression and function *in vivo*

To investigate a possible role of MMA arginine in mRNA metabolism in *Leishmania* parasites, the N-termini of select target RBPs were endogenously HA-tagged, leaving 3′*UTR*s intact as transcript stability and translational control are overwhelmingly 3′*UTR*-driven (8,42). Wild-type and *Δprmt7* parasites were engineered to express HA-tagged Alba3, RBP16, Torus and DDX3 RBPs (Supplementary Figure S2). Torus is a CCCH-type zinc finger protein with a conserved Torus domain that, like DDX3 (HEL67) (43), co-immunoprecipitates with PRMT7 (10).

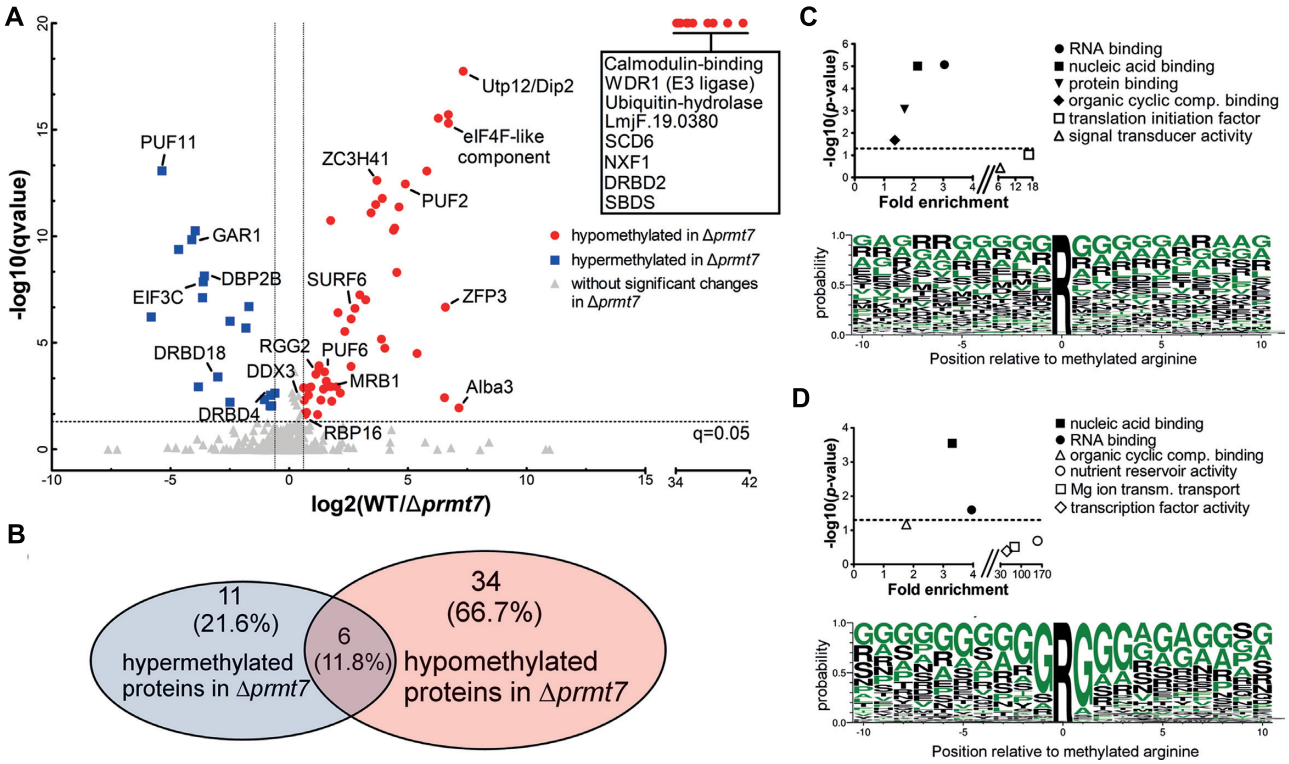

Figure 2. RNA-binding proteins are putative substrates for PRMT7 arginine monomethylation. (**A**) Methyl-SILAC peptide pairs were analyzed according to their methylation status in WT versus Δ*prmt7 Leishmania major* cells. Mass spectra quantification of each light and heavy pair ratios detected peptides with increased (hypermethylated, in blue) or decreased (hypomethylated, in red) methylation in *Δprmt7* as compared to WT. Methylated RNA-binding proteins (RBPs) are shown as well as proteins that had no methyl peptides detected in *Δprmt7* (boxed RBPs). Of 247 identified proteins with isolated MMA peptides, 62 are RBPs; 17 of which are hypomethylated in *Δprmt7* (Hochberg and Benjamini test $q < 0.05$). (**B**) 51 proteins are differentially methylated between WT and *Δprmt7*; 6 of which are both hypomethylated and hypermethylated at different residues. (**C, D**) Significantly enriched Molecular Function Gene Ontology (GO) Terms (upper panel) and selected amino acid residues (lower panel) in the whole MMA proteome (C) versus *Δprmt7* hypomethylated proteins (**D**). For the global data, RNA binding was highlighted (upper panel), yet there is no clear consensus MMA site sequence (lower panel). RNA binding remains characteristic of Δ*prmt7* hypomethylated proteins, and an enrichment for the 'RGG' motif is evident (lower panel). Dotted lines in upper panels depict Bonferroni *P*-value = 0.05.

Examination of HA-Torus, HA-RBP16 and HA-DDX3 levels in WT and *Δprmt7* promastigote cells at log and stationary stages show that these RBPs are differentially expressed in the absence of PRMT7 levels (Figure 5A). Both HA-Torus and HA-RBP16 have reduced expression *in Δprmt7* parasites, the former at both log and stationary phase, the latter only in stationary promastigotes. In contrast, HA-DDX3 is slightly upregulated in *Δprmt7* at stationary phase with potential degradative products evident. The detection of a smaller HA-DDX3 band of ∼30 kDa at the stationary phase suggests enzymatic cleavage, a possible sign of protein instability and coordinated control of expression. The observation that these RBP protein levels are altered in Δ*prmt7* relative to wildtype stationary phase cells (Figure 5A) is interesting as PRMT7 expression is tightly downregulated prior to this lifecycle stage (10). The stage-specific eradication of RBP16 levels in the Δ*prmt7* mutant cells was therefore examined in two different but complementary experimental contexts.

To determine whether reduced HA-RBP16 levels in *Δprmt7* cells are due to expedited protein decay rates or reduced translation of *rbp16* transcript, the protein stability of both RBP16 and Alba3 was assessed in WT versus Δ*prmt7* cells (Figure 5B and Supplementary Figure S3). Of note, the half-life of HA-RBP16 is reduced specifically in stationary phase Δ*prmt7* cells relative to WT background or log phase (Figure 5B). Densitometry analysis revealed HA-RBP16 protein half-life is >6 h in WT and 0.86 h in Δ*prmt7* cells at stationary phase (Figure 5B and Supplementary Figure S3B). In contrast, stability of HA-Alba3 protein was unchanged between samples (Supplementary Figure S3). This suggests PRMT7-dependent methylation can post-translationally control select target protein degradation rates in a stage-specific manner.

To determine whether the half-life of HA-RBP16 was impacted by subcellular localization, N-terminally tagged HA-RBP16 was examined using immunofluorescence. Similar to immunoblot results (Figure 5A, Supplementary Figure S4B), the HA-RBP16 protein signal specifically decreases in *Δprmt7* promastigotes at stationary phase (Supplementary Figure S4E). Unlike the close RBP16 orthologue in *T. brucei, Tb*RBP16 (38,44), N-terminally tagged HA-RBP16 localises in the cytoplasm and does not appear to traffic to the mitochondria (Supplementary Figures S4C and E). Cytoplasmic localization of HA-Alba3 was unaltered between promastigotes samples (Supplementary Figure S4F). We therefore examined the subcellular localization and relative stability of endogenous *Lmj*RBP16 using

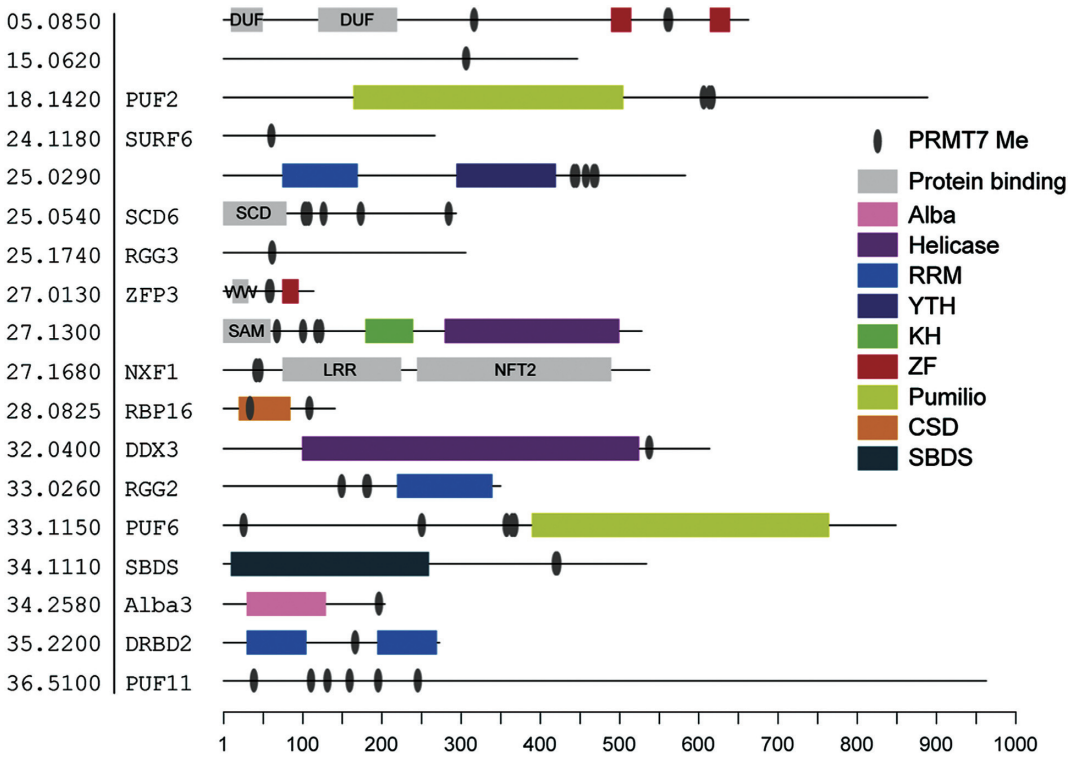

Figure 3. Monomethyl arginines are found outside RNA-binding domains. Bioinformatic analysis of 18 PRMT7 targets showing sites where MMA was detected and the predicted locations of different classes of RNA- or protein-binding domains. RNA-binding domains are colour coded (see legend) while protein-binding domains are annotated and shown in gray. Regions lacking an identifiable domain or with predicted disorder are shown by a solid line. Domain annotations: DUF, domain of unknown function; KH, K homology; LRR, Leucine-rich repeat; LSm, like Smith antigen; NFT2, nuclear transport factor 2; SAM, sterile alpha motif; SBDS, Shwachman–Bodian–Diamond syndrome protein; YTH, YT521-B homology. Positions of domain boundaries and methylated arginines are relative to the scale bar. Entries ordered by TriTrypDB gene identifier. Protein names provided where assigned.

anti-*Tb*RBP16 (kind gift of L. Read), and found that while the HA-RBP16 protein is cytoplasmic, untagged endogenous *Lmj*RBP16 is indeed mitochondrial (Supplementary Figures S4C and D). We tested the subcellular localization of C-terminally-tagged endogenous RBP16-HA and found it is also mitochondrial (data not shown). This suggests N-terminal HA tagging of *Lmj*RBP16 is sufficient to disrupt proper mitochondrial localization. Of note, neither the mitochondrial-localised endogenous *Lmj*RBP16 or endogenously tagged *Lmj*RBP16-HA are destabilized in the stationary cell stage in the absence of PRMT7 levels (Supplementary Figure S4A). As the *rbp16* transcript is nuclear-derived and cytoplasmically translated, there is biological relevance to the relative stability of this potential metabolic regulator in the cytoplasm. This provides two useful mechanistic insights, firstly that PRMT7 methylation can shield a cytoplasmic RBP from protein degradation in an *in vivo* context and secondly that the protein degradation is distinct between cytoplasmic and mitochondrial cellular compartments and between lifecycle stages.

PRMT7-mediated methylation modulates post-transcriptional gene control

Unexpectedly, endogenous levels and subcellular localization of HA-Alba3 remain constant despite removal of PRMT7 expression (Figure 6A, Supplementary Figure S4D). We generated hypomethylated Alba3^{WGG}, HA-Alba3^{KGG} and HA-Alba3^{R192K} heterozygous mutants with RGG methyl sites replaced by WGG or KGG in the protein C-terminus to evaluate target specificity. In contrast to other RBPs investigated, there were no changes in either endogenously tagged HA-Alba3^{WT}, HA-Alba3^{WGG}, HA-Alba3^{KGG} or HA-Alba3^{R192K} protein levels in the absence of PRMT7 levels (Figures 6A and 7A). Immunoprecipitation of HA-Alba3 and probing with anti-MMA revealed that monomethylation is only detected in WT cells and absent in all mutant HA-Alba proteins expressed in both WT and Δ*prmt7* cell lines (Figures 6B and 7B), validating the C-terminal RGG motifs, and isolating R192 as necessary for *in vivo* Alba3 methylation by PRMT7. Therefore, we investigated the potential influence of arginine methylation on Alba3 mRNA-binding function.

Previously, *Li*Alba3 has been shown to bind to δ-*amastin* (*LinJ.34.1010*) and *p1/s1 nuclease* (*LinJ.30.1520*) transcripts in *Leishmania infantum* cells (36). Therefore, we tested whether Alba3 RNA-binding is conserved and impacted by PRMT7-dependent methylation. Promastigotes cells were UV-crosslinked *in vivo* followed by anti-HA RNA immunoprecipitation (RIP) to isolate HA-Alba3 mRNP complexes and specific transcript targets were quantified by qRT-PCR. Remarkably, endogenous HA-Alba3 showed differential RNA-binding affinity in the absence of PRMT7-dependent methylation. The *in vivo* interaction of Alba3 with stage-regulated mRNAs δ-*amastin*

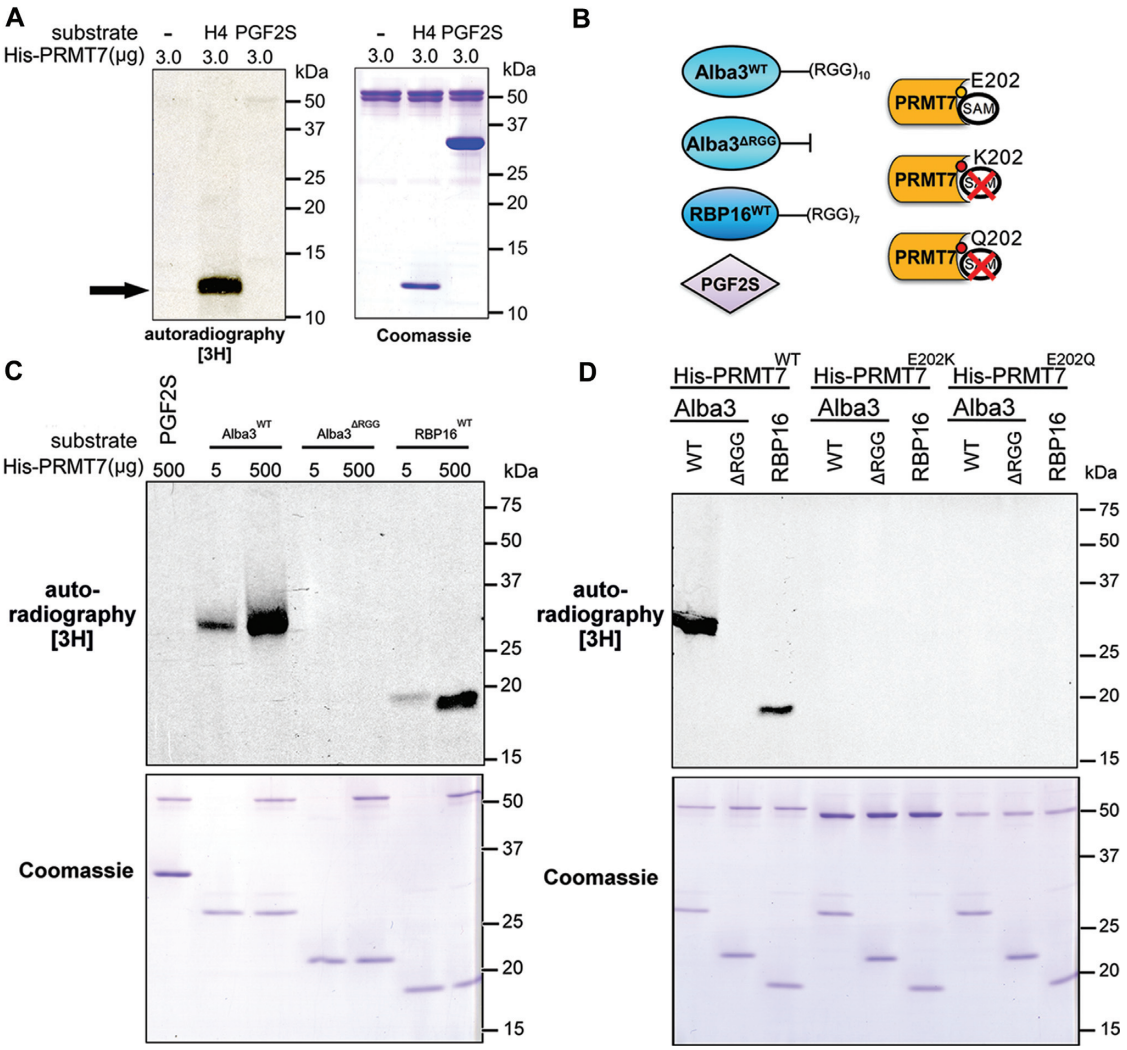

Figure 4. *In vitro* methylation of Alba3 and RBP16 by PRMT7. (**A**) Recombinant His-PRMT7 was tested for methyltransferase activity *in vitro* in the presence of radioactive methyl donor *S*-adenosyl methionine, human histone H4 as (1 μg) a canonical RGG-containing PRMT substrate (black arrow) and a *Leishmania braziliensis* protein rich in arginines but devoid of RGG motifs as a negative control (*Lbr*PGF2S). (**B**) Purified His-tagged PRMT7 putative substrates Alba3^{WT}, RBP16^{WT} and RGG-deficient Alba3$^{\Delta RGG}$ were tested, as well as *Lbr*PGF2S^{WT}. PRMT7 E202 residue in the double E loop motif was mutated to K or Q to generate catalytically-inactive mutants. (**C**) RNA-binding proteins Alba3^{WT} and RBP16 are arginine methylated by PRMT7 *in vitro*, while Alba3$^{\Delta RGG}$ and LbrPGF2S^{WT} are not. (**D**) *In vitro* methylation of target RBPs by PRMT7 is disrupted by mutating residue E202 (PRMT7^{E202K} and PRMT7^{E202Q}). Coomassies demonstrate relative loading.

(*LmjF.34.0500*) and *p1/s1 nuclease* (LmjF.30.1510) is dependent on methylation by PRMT7 (Figures 6C, D and 7C). In contrast, Alba3 binding to the constitutively-expressed *nmt* (*N-myristoyltransferase*) and *gapdh* mRNA targets is not altered by PRMT7 knockout. While total δ-*amastin* expression levels are reduced in *Δprmt7*, *nmt* transcript levels are constant, suggesting divergent regulatory mechanisms between the two transcripts (Figure 6D).

To further analyze Alba3 binding to δ-*amastin*, HA-Alba3^{WT}, HA-Alba3^{WGG}, HA-Alba3^{R192K} and HA-Alba3^{KGG} mRNPs were purified from WT and Δ*prmt7* samples and quantified by qRT-PCR. Interaction between Alba3 and δ-*amastin* mRNA is consistently inhibited in Δ*prmt7* cells *in vivo* (Figures 6C, D and 7C). This interaction was disrupted in HA-Alba3^{WGG} and HA-Alba3^{KGG} (Figures 6D and 7C), corroborating the role of C-terminal tail methylation upon Alba3 RNA-binding capacity. As a control, *nmt* mRNA associates with Alba3 at similar levels in WT and Δ*prmt7* cells and *nmt* transcript stability is unchanged (Figures 6C–E and 7C). Notably, while the specific mutation of arginine 192 to a lysine (R192K) was sufficient to ablate Alba3 MMA by PRMT7 *in vivo*, this does not disrupt Alba3 association with δ-*amastin* or *nmt*, but is sufficient to disrupt association with *p1s1* target transcript (Figure 7C). Indeed, the trypsin digest of proteins prior to isolation of monomethylated peptides may have disrupted the proper identification of multiple RGG motif-containing peptides from within the Alba3 C-terminus, and possibly other target proteins. This suggests Alba3 association with δ-*amastin* mRNA may require PRMT7-dependent monomethylation of C-terminal RGG motifs in addition to R192.

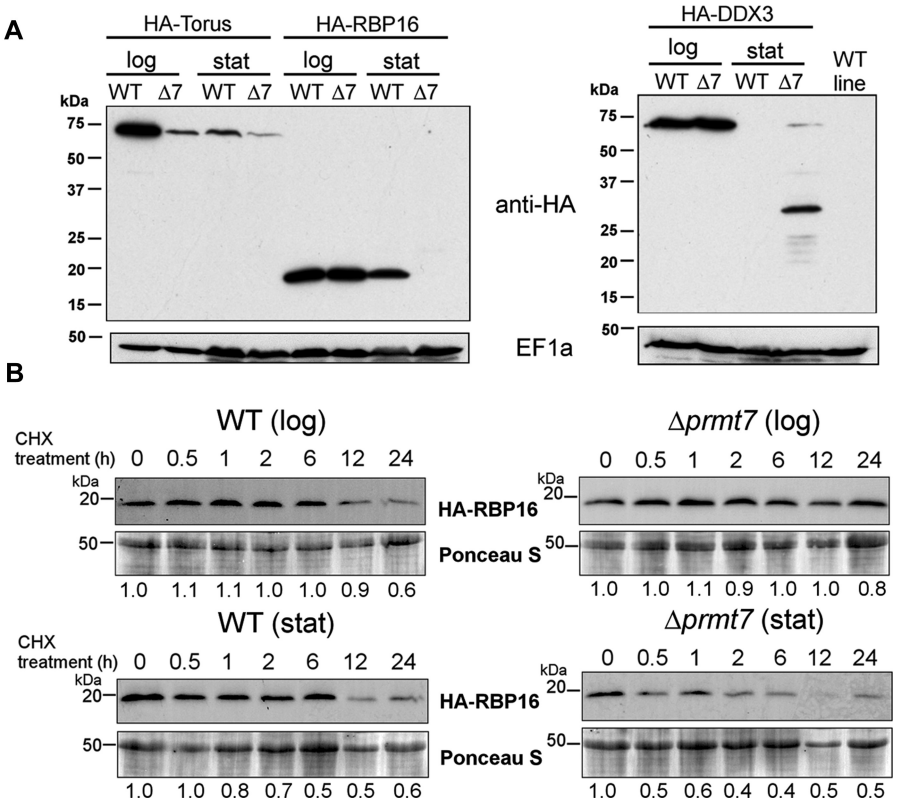

Figure 5. PRMT7 knockout affects target RBP expression *in vivo*. (**A**) Expression levels of three endogenously-tagged RBPs, Torus, RBP16 and DDX3, are altered in *Δprmt7* (Δ7) parasites. Lanes are labeled for logarithmic (log) versus stationary (stat) phase promastigotes. EF1a levels are shown as a loading control. (**B**) HA-RBP16 protein stability was analyzed in log and stationary promastigotes after cycloheximide (CHX) addition. Ponceau staining is shown as loading control. HA-RBP16/Ponceau ratio values are shown below each lane. HA-RBP16 protein half-life was >6 h in WT cells and 0.86 h in Δ*prmt7* according to a one-phase and a two-phase decay exponential fit, respectively.

It has been reported that Alba3 participates in the stabilization of δ-*amastin* mRNAs in *L. infantum* (36). We thus investigated whether PRMT7-mediated methylation affects δ-*amastin* transcript stability. Samples from cells treated with actinomycin to block transcription, revealed that δ-*amastin* is only stabilized when Alba3 is monomethylated (Figures 6E and 7C). Either PRMT7 knockout or expression of hypomethylated Alba3 resulted in a significant decrease of δ-*amastin* mRNA half-life from 3.8 h in WT to 0.95 h in Δ*prmt7* (Figure 6E). Collectively, this indicates PRMT7-dependent MMA methylation of Alba3 impacts RNA binding in a target-specific manner. In summary, our data demonstrate methylation by PRMT7 can regulate the relative protein stability and selective RNA affinity of distinct RBP targets.

DISCUSSION

To date, a limited number of arginine methylated proteins have been identified in *Leishmania* spp. (10,45). In this study, we report that 3% (∼247) of the entire *L. major* predicted proteome carries at least one monomethylated arginine (20). This number of MMA-targeted proteins is relatively large considering arginines can also be dimethylated and since other post-translational modifications (PTMs) have been detected in *Leishmania* spp., including ∼600 phosphorylated proteins (7%) (46). We demonstrate that PRMT7-dependent methylation strongly impacts the MMA proteome of *L.major* parasites thus regulating RBP expression and/or function (Figure 8). Notably, PRMT7 levels regulate the expression levels of three isolated RBP targets in at least one developmental stage (Figure 5A), suggesting that arginine methylation can affect protein turnover in *Leishmania* spp.

Overall, experimental evidence indicates *Leishmania major* PRMT7 activity impacts protein target stability (Figure 5) and function (Figures 6 and 7) in a context-dependent manner, distinct from that of mammalian homologs. Despite not being an essential protein in *L. major,* PRMT7 levels regulate leishmaniasis disease pathology (10). Remarkably, epigenetic control by PRMT7-dependent monomethylation of the primary gene regulators in this system, RBPs, mediates virulence of the human-infective lifecycle stage four differentiation events downstream of PRMT7 expression. This undermines the traditional paradigm that influential *trans*-regulators are temporally synchronized with the cellular processes they promote and provides another layer of depth to the complexities of *Leishmania* genetics.

Interestingly, 17 proteins are hypermethylated in *Δprmt7* parasites (Figure 2A and B). This and the viability of *Δprmt7* parasites may suggest modulation of alternative PRMT activity to functionally compensate for PRMT7 depletion. Six of the hypermethylated proteins also contain distal sites which are hypomethylated; indicative of a

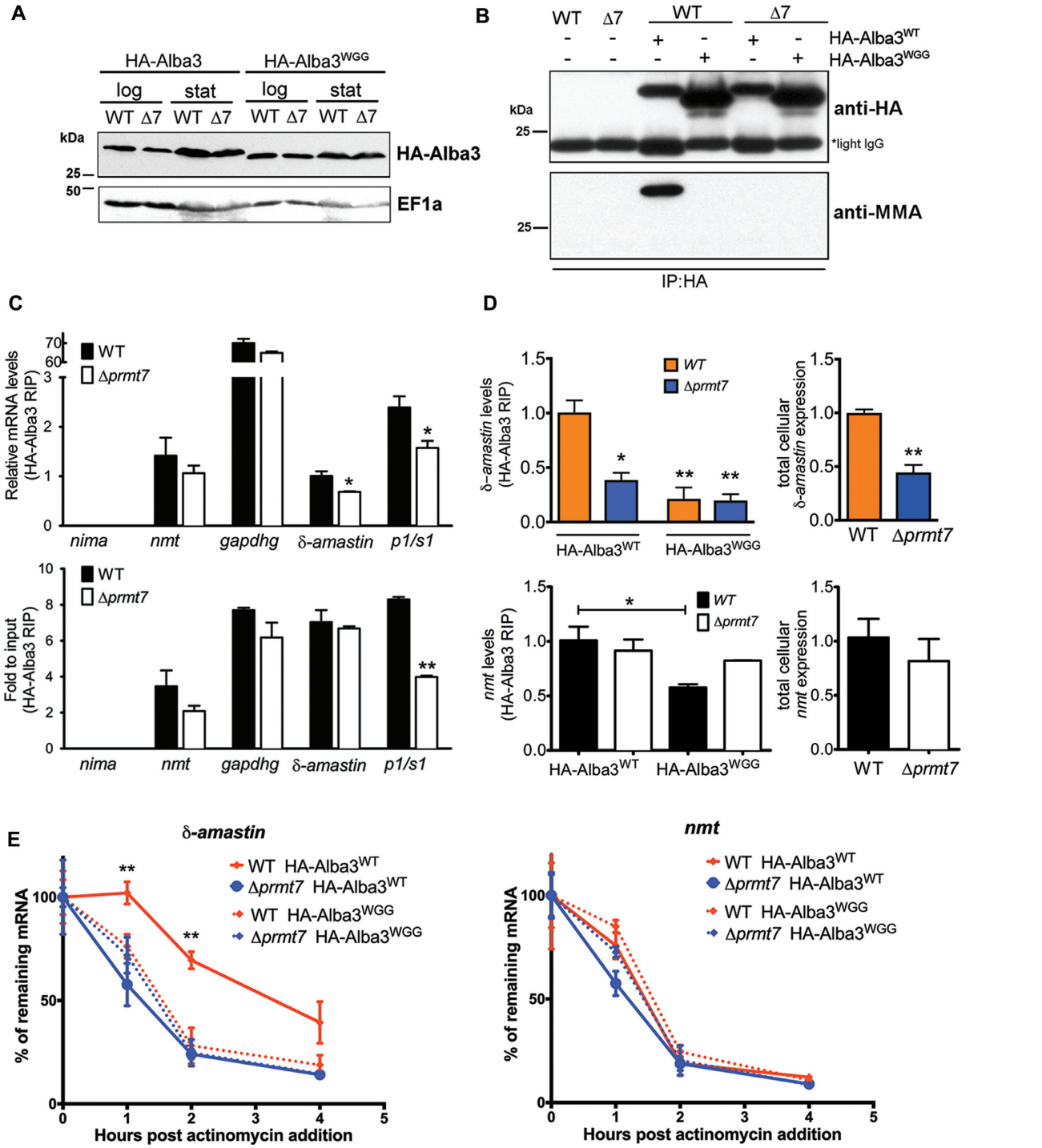

Figure 6. Arginine methylation of Alba3 contributes to mRNA binding and δ-*amastin* stabilization. (**A**) Endogenously tagged Alba3^{WT} and RGG→WGG hypomethylated mutant (Alba3^{WGG}) showed no differential expression levels between WT and Δ*prmt7* cells. The migration of HA-Alba3^{WGG} mutant protein is faster on SDS-PAGE, independent of PRMT7 levels. (**B**) Immunoprecipitation of HA-Alba3 shows loss of arginine monomethylation in Δ*prmt7* parasites and when the C-terminal RGG motifs are mutated into WGG. (**C**) Alba3 complexes were purified by RNA co-immunoprecipitation (RIP) from *in vivo* UV-crosslinked cell lysates. Eluted RNA are analyzed by qRT-PCR and suggest that δ-*amastin* and *p1/s1* nuclease, but not *gapdhg* or *nmt* transcript binding to Alba3 decreases in the absence of PRMT7 levels. RIP transcript levels are relative to 18S rRNA in upper panel and lower panel are relative to total cellular levels (input). $*P < 0.05$, Bonferroni two-way ANOVA test. (**D**) qRT-PCR analysis of δ-*amastin* (upper panels) *and nmt* (lower panels) mRNA association to HA-Alba3 and HA-Alba3^{WGG} mutant. Quantification of HA-Alba3 RIP eluted transcripts (left panel) and total input RNA (right panel) is shown. $*P < 0.05$, $**P < 0.01$, Tukey one-way ANOVA test (left panel) and unpaired two-tailed *t*-test (right panel). (**E**) Stability of δ-*amastin* (left panel) and control *nmt* (right panel) transcripts were evaluated in wild-type (WT) and Δ*prmt7* after actinomycin treatment. RNA samples from cells expressing wild-type (Alba3^{WT}) or hypomethylated (Alba3^{WGG}) Alba3 were used in qRT-PCR. δ-*amastin* mRNA half-life was >3.8 h in WT and 0.95 h in Δ*prmt7* cells expressing HA-Alba3^{WT}, and, respectively, 1 and 1.2 h for HA-Alba3^{WGG}. Transcript levels were normalized against 18S rRNA and are plotted as mean ± standard error of two biological replicates. $**P < 0.01$, Bonferroni two-way ANOVA test.

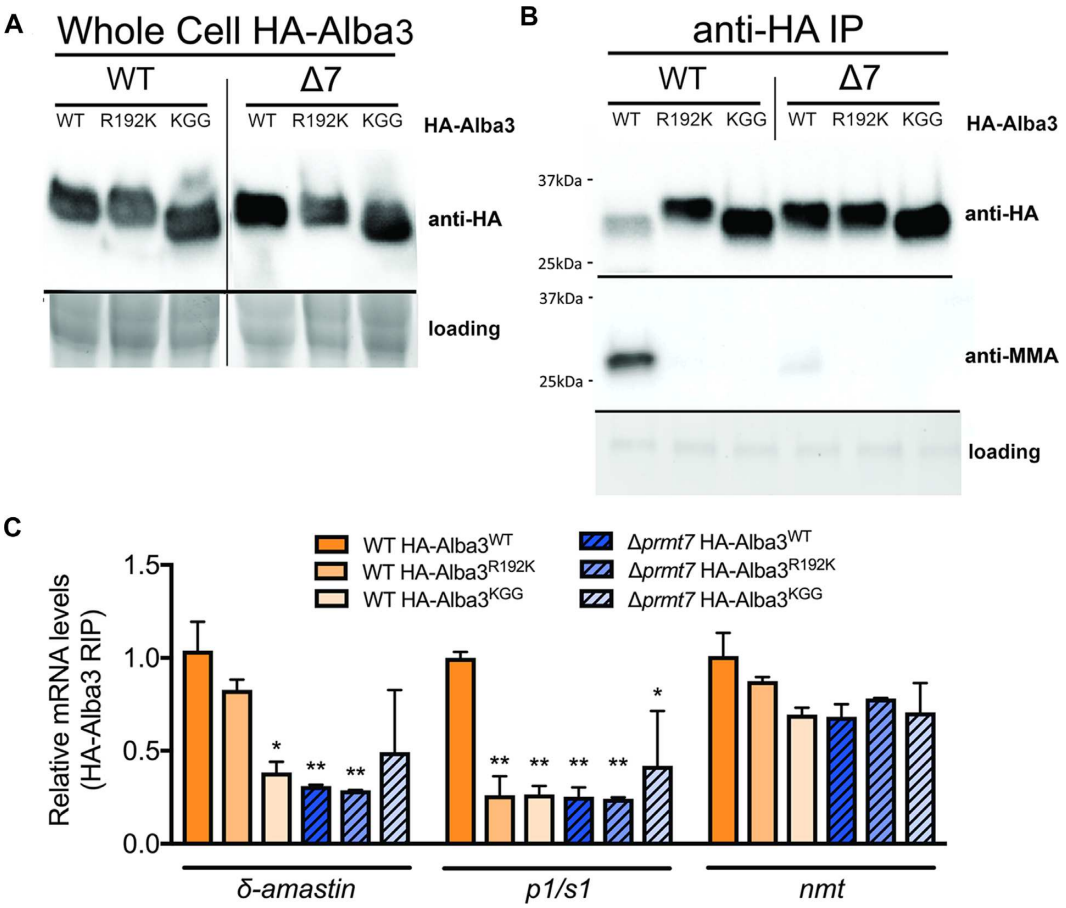

Figure 7. Arginine methylation of Alba3 contributes to binding of *δ-amastin* and *p1s1* mRNAs. (**A**) Endogenously tagged Alba3^{WT}, RGG→KGG single point mutant (Alba3^{R192K}) and hypomethylated mutant (Alba3^{KGG}) showed no differential expression levels between WT and *Δprmt7* cells. The migration of HA-Alba3^{KGG} mutant protein is faster on SDS-PAGE, independent of PRMT7 levels. (**B**) Immunoprecipitation of HA-Alba3 shows arginine monomethylation is ablated in the RGG→KGG single point mutant (Alba3^{R192K}), when all C-terminal RGG motifs are mutated into KGG (HA-Alba3^{KGG}) and in *Δprmt7* parasites. (**C**) Alba3 complexes were purified by RNA co-immunoprecipitation from *in vivo* UV-crosslinked cell lysates. Eluted RNA were analyzed by qRT-PCR and confirm that Alba3 binding to *δ-amastin* and *p1/s1* nuclease decreases in the absence of PRMT7, but Alba3:*nmt* association remains constant independent of R mutation or PRMT7 levels. Interestingly, mutation of R192K disrupts Alba3:*p1s1* association, but only mildly impacts Alba3:*δ-amastin* binding. Transcript levels are relative to 18S rRNA. $*P < 0.05$, $**P < 0.01$, Bonferroni two-way ANOVA test.

complex PRMT inter-regulatory system. Deletion of mammalian PRMT1, which catalyzes asymmetric dimethylarginine (43), results in an increase of global MMA in mammals and *T.brucei* (47,48). Therefore, functional overlap between *Leishmania* PRMTs may involve a dynamic regulatory interplay as it does in *T.brucei* (49). A unique example of substrate competition by PRMTs in human cells is regulation of transcription elongation factor E2F-1-mediated apoptosis by arginine methylation (50). Here, PRMTs determine apoptotic outcomes by competing for the same E2F-1 substrate; SDMA methylation by PRMT5 leads to apoptosis in DNA damaged cells, while ADMA methylation by PRMT1 favors proliferation. The detection of PRMT3 MMA peptides in our isolates (*LmjF.03.0600*; Supplementary Table S1) further supports methyltransferase inter-regulation. While PRMT3 is catalytically inactive in *T. brucei* due to the absence of key residues in the SAM-binding domain (51), the two essential glutamate residues in the double-E loop are still present in *Leishmania* (Supplementary Figure S1), suggesting a different regulatory role for *Lmj*PRMT3. This exciting distinction suggests PRMT3 may be a functional enzyme rather than a prozyme in *Leishmania*.

Arginine methylation sites vary considerably according to the PRMT enzyme or the organism investigated (2). RG and RXR sites represent the majority of mammalian PRMT target motifs but there are exceptions (41). Our methyl-SILAC analysis identified RG/RGG as the main target for PRMT7 methylation *in vivo*. Conserved protein domain analysis revealed that most of PRMT7-dependent methylation is not found directly within classical RNA-binding domains (Figure 3). Of interest, despite the capacity to modify H4 *in vitro* (Figure 4A), no histone MMA peptides were identified by our screen (Figure 2A, Supplementary Table S1). This could be due to the cytoplasmic-specific localization of *Lmj*PRMT7, methodological limitations or a low overall abundance of MMA in *Leishmania* histone proteins.

Although arginine methylation has been mostly associated with changes in protein-protein interactions (2), there are multiple examples of direct modulation of RNA-protein binding in mammalian cells (52–54). PRMTs have previously been shown to regulate the RNA affinity of target

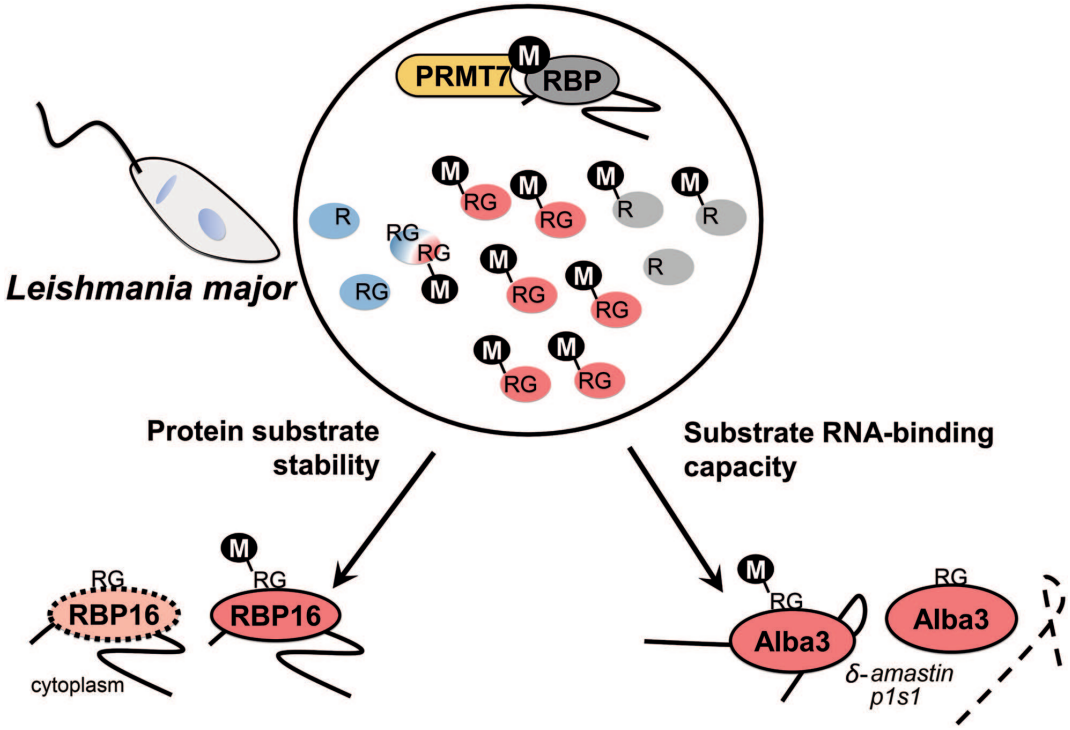

Figure 8. PRMT7 regulates RNA-binding protein function in *Leishmania*. Overview diagram describing the putative role of PRMT7-dependent methylation based on the effects of *L. major* PRMT7 knockout upon the arginine methylation of selected RBPs. Red circles represent RBPs hypomethylated in Δ*prmt7*, while blue are hypermethylated. PRMT7 contributes to the protein stability of cytoplasmic RBP16 in stationary promastigotes and to Alba3 RNA-binding affinity *to* δ-*amastin* and *p1/s1* nuclease mRNAs. Hypomethylation of Alba3 consequently results in decreased *δ-amastin* half-life.

RBPs in other systems (55,56). In *T. brucei*, the RNA-binding proteins DRBD18 and PRMT1 have been shown to modulate the fate of mRNAs according to methylation state, impacting both protein and mRNA binding (51,57). Here, we dissect the effect of MMA upon RNA affinity and isolate the specific arginines of Alba3 that are monomethylated by PRMT7; resulting in the discrete maintenance or loss of specific transcript targets. In line with the previous finding that *L. infantum* Alba3 stabilizes δ-*amastin* transcripts (36), we find that overall δ-*amastin* levels are significantly reduced in the Δ*prmt7* mutant *L. major* lines. This indirect regulation of δ-*amastin* by PRMT7 levels is most likely due to reduced association with the hypomethylated Alba3. Amastins are thought to function as membrane transporters and are largely regarded as important virulence factors in *Leishmania* species as reduced levels of δ-*amastins* via gene knockdown limits pathogenesis of infection in mice (58).

Our results indicate arginine monomethylation of the Alba3 C-terminus increases binding to *δ-amastin* and promotes transcript stabilization (Figures 6C-E and 7C). Unlike δ-*amastin*, expression levels of *p1/s1 nuclease* Alba3 target transcript are not altered by PRMT7 levels, although arginine methylation of Alba3 R192 is necessary for association (Figure 7C). In contrast, Alba3 transcript target *nmt* is not impacted by PRMT7 levels (Figures 6C–E and 7C). These results suggest Alba3 regulates mRNA fate in a highly bespoke and transcript-specific manner. There is a low correlation between protein expression and mRNA binding capacity of RBPs and mRNPs display context-dependent selection of components in *Leishmania* (8). Further investigation of the molecular requirements and functional impact of RBP modification is therefore crucial to understanding gene regulation not only in *Leishmania*, but all eukaryotes.

The impact of PTM upon RNA binding potential may be indirect. The CCCH zinc finger protein ZFP3 is known to associate with ZFP1 in *T.brucei* and this interaction is necessary for both RNA target specificity as well as polysomal association (59). Here, we identify ZFP3 as a target of PRMT7-dependent MMA in *Leishmania* (Figure 2A). It is possible a ZFP3:ZFP1 interaction could be impacted by the presence of methylarginine altering both the RBP spatial proximity and RNA target binding. *In silico* docking analyses suggest several residues in the Alba domain are buried inside the Alba3:Alba1 heterodimeric protein complex but the RGG motif in the C-terminal tail is exposed (60). Consistent with the absence of RGG motifs, the Alba1 protein was not detected in our methyl-SILAC analysis. It is not known whether methylation of the Alba3 RGG tail regulates the stress-induced localization of the Alba proteins (37). Proper characterization of MMA target RBP structural dynamics is necessary to determine the impact of methylation on mRNP complex assembly.

Unusually, PRMT7-dependent methylation promotes the stability of cytoplasmic RBP16 protein beyond the temporal expression of PRMT7 protein levels (Figure 5 and Supplementary Figure S4). The regulation of protein turnover observed represents a novel function for PRMT7-dependent methylation (Figure 5). *T. brucei* RBP16 was

the first Y-box protein to be found in mitochondria, where it associates with guide RNAs (gRNAs) and has a role in mitochondrial mRNA editing (29,38). The N-terminal cold-shock domain and RGG-rich C-terminus of *Tb*RBP16 both contribute to RNA-binding capacity (61). Arginine residues in the *T. brucei* RBP16 C-terminus are targeted by PRMT1 methylation, impacting RNA editing complexes (38). We find that RBP16 in *Leishmania* is also mitochondrial and this localization is not affected by the absence of PRMT7 (Supplementary Figure S4B). However, the N-terminal tagging of endogenous RBP16 protein renders it cytoplasmic, where the RBP half-life is specifically reduced in Δ*prmt7* knockout cells in a human-infective stage (Figure 5, Supplementary Figure S4C). This reduced stability suggests protein degradation can be inhibited in wild-type cells via PRMT7-dependent methylation, which is particularly interesting at a lifecycle stage at which PRMT7 is not expressed. This lends insight into the distinct cellular microenvironments influencing protein degradation in cytoplasm versus mitochondria to impact RBP function and stability. Potential mechanisms include inhibition of protein ubiquitination and proteasome degradation targeting. Cytoplasmic protein turnover rate is largely regulated by the ubiquitin–proteasome system and polyubiquitination is the classical marker for this pathway (62). Interdependent ubiquitination and methylation has been detected previously in other systems (63,64). In mammalian innate immune response, TNF receptor-associated 6 (TRAF6) ubiquitin ligase activity is inhibited by PRMT1 methylation (64). Activation of Toll-like receptor response leads to hypomethylated TRAF6 via demethylation by JMJD6 and downregulation of PRMT1 expression. This triggers TRAF6 ubiquitin ligase activity and NF-kB response. In *L. major*, a putative JMJD6 demethylase ortholog gene may enable dynamic arginine methylation in protozoa (Tritrypdb.org). To fully understand the function of RBP16 in these parasites we must examine other PTMs controlling RBP16 function.

The Lsm domain-containing SCD6 is another protein with simultaneous identification of hypo- and hypermethylated sites (Figure 2A and Supplementary Table S1). This RBP is involved in processing body (P-body) granule formation in *T. brucei*; specifically responsible for coordinating granule assembly (65). Sequential deletion of the *Tb*SCD6 RGG motifs, orthologous to targets of PRMT7 methylation identified by our *Leishmania* screen, led to a proportional decrease in RNA granule numbers in *T. brucei*. This suggests arginine methylation may play a crucial role in controlling the fate of all mRNPs in the cell; impacting both mRNA metabolism and sequestration. At least four other methylated RBPs have been shown to co-purify with RNA granules in *T. brucei*: DDX3, PABP1, DRBD4 and Alba3 (66).

In conclusion, we introduce *Leishmania* as a model organism to specifically study PRMT activity and functional impact of methylation upon non-histone targets. We explore methyl-SILAC as a productive, verified approach to investigate protozoa PRMT function and target isolation. Our data indicate that PRMTs have a central role in mRNA metabolism control by modulating the stability and function of post-transcriptional regulators in *Leishmania*. PRMT7 activity thus has a demonstrated role in gene expression control, both directly at the post-translational level and indirectly at the post-transcriptional level. Taken together, our data indicate the *Leishmania* PRMT7-directed regulatory pathway epigenetically controls parasite gene expression long after PRMT7 expression.

SUPPLEMENTARY DATA

Supplementary Data are available at NAR Online.

ACKNOWLEDGEMENTS

We thank Profs. Deborah Smith, Jeremy Mottram and Dawn Coverley for thoughtful comments on this manuscript. We thank Drs. James Brannigan, Jaspreet Grewal, Vincent Geoghegan, Juliana Diniz, Sarah Forrester and Luis de Pablos for helpful discussions on the *Leishmania* SILAC labeling and methyl-SILAC data analysis. We thank Dr. Suzanne McDermott for helpful discussion on RBP16 and Prof. Laurie Read for anti-*Tb*RBP16 antibody. Proteomic and RNA identification and analyses were conducted in the MAP and Genomics and Bioinformatics Labs, respectively, in the Bioscience Technology Facility at the University of York (https://www.york.ac.uk/biology/technology-facility).

FUNDING

Newton Fund; Medical Research Council [MR/M02640X/1, MR/N017633/1]; Sao Paulo Research Foundation [FAPESP 2014/19400-1, MRC/FAPESP 2015/13618-8, 2014/50954-3]; Brazilian National Council for Scientific and Technological Development (CNPq) [PDE 234480/2014-9]; LCMS within the York Centre of Excellence in Mass Spectrometry was supported through Science City York, Yorkshire Forward/Northern Way Initiative; EPSRC [EP/K039660/1, EP/M028127/1]. Funding for open access charge: University of York Library, Medical Research Council research grant.
Conflict of interest statement. None declared.

REFERENCES

1. Jarrold,J. and Davies,C.C. (2019) PRMTs and arginine methylation: cancer's best-kept secret? *Trends Mol. Med.*, **25**, 993–1009.
2. Guccione,E. and Richard,S. (2019) The regulation, functions and clinical relevance of arginine methylation. *Nat. Rev. Mol. Cell Biol.*, **20**, 642–657.
3. Geoghegan,V., Guo,A., Trudgian,D., Thomas,B. and Acuto,O. (2015) Comprehensive identification of arginine methylation in primary T cells reveals regulatory roles in cell signalling. *Nat. Commun.*, **6**, 6758.
4. Fisk,J.C., Sayegh,J., Zurita-Lopez,C., Menon,S., Presnyak,V., Clarke,S.G. and Read,L.K. (2009) A type III protein arginine methyltransferase from the protozoan parasite Trypanosoma brucei. *J. Biol. Chem.*, **284**, 11590–11600.
5. Jain,K. and Clarke,S.G. (2019) PRMT7 as a unique member of the protein arginine methyltransferase family: A review. *Arch. Biochem. Biophys.*, **665**, 36–45.
6. Karkhanis,V., Wang,L., Tae,S., Hu,Y.J., Imbalzano,A.N. and Sif,S. (2012) Protein Arginine Methyltransferase 7 Regulates Cellular Response to DNA Damage by Methylating Promoter Histones H2A and H4 of the Polymerase delta Catalytic Subunit Gene, POLD1. *J. Biol. Chem.*, **287**, 29801–29814.
7. De Pablos,L.M., Ferreira,T.R. and Walrad,P.B. (2016) Developmental differentiation in Leishmania lifecycle progression:

post-transcriptional control conducts the orchestra. *Curr. Opin. Microbiol.*, **34**, 82–89.
8. de Pablos,L.M., Ferreira,T.R., Dowle,A.A., Forrester,S., Parry,E., Newling,K. and Walrad,P.B. (2019) The mRNA-bound proteome of leishmania mexicana: Novel genetic insight into an ancient parasite. *Mol. Cell Proteomics*, **18**, 1271–1284.
9. Alvar,J., Velez,I.D., Bern,C., Herrero,M., Desjeux,P., Cano,J., Jannin,J. and den Boer,M. (2012) Leishmaniasis worldwide and global estimates of its incidence. *PLoS One*, **7**, e35671.
10. Ferreira,T.R., Alves-Ferreira,E.V., Defina,T.P., Walrad,P., Papadopoulou,B. and Cruz,A.K. (2014) Altered expression of an RBP-associated arginine methyltransferase 7 in Leishmania major affects parasite infection. *Mol. Microbiol*, **94**, 1085–1102.
11. Herrmann,F., Pably,P., Eckerich,C., Bedford,M.T. and Fackelmayer,F.O. (2009) Human protein arginine methyltransferases in vivo–distinct properties of eight canonical members of the PRMT family. *J. Cell Sci.*, **122**, 667–677.
12. Bates,P.A. (2018) Revising Leishmania's life cycle. *Nat. Microbiol.*, **3**, 529–530.
13. Yang,Y. and Bedford,M.T. (2013) Protein arginine methyltransferases and cancer. *Nat. Rev. Cancer*, **13**, 37–50.
14. Larsen,S.C., Sylvestersen,K.B., Mund,A., Lyon,D., Mullari,M., Madsen,M.V., Daniel,J.A., Jensen,L.J. and Nielsen,M.L. (2016) Proteome-wide analysis of arginine monomethylation reveals widespread occurrence in human cells. *Sci. Signal.*, **9**, rs9.
15. Rogers,M., Kropf,P., Choi,B.S., Dillon,R., Podinovskaia,M., Bates,P. and Muller,I. (2009) Proteophosophoglycans regurgitated by Leishmania-infected sand flies target the L-arginine metabolism of host macrophages to promote parasite survival. *PLoS Pathog.*, **5**, e1000555.
16. Fulwiler,A.L., Soysa,D.R., Ullman,B. and Yates,P.A. (2011) A rapid, efficient and economical method for generating leishmanial gene targeting constructs. *Mol. Biochem. Parasitol.*, **175**, 209–212.
17. Hart-Smith,G., Yagoub,D., Tay,A.P., Pickford,R. and Wilkins,M.R. (2016) Large scale mass Spectrometry-based identifications of Enzyme-mediated protein methylation are subject to high false discovery rates. *Mol. Cell Proteomics*, **15**, 989–1006.
18. Aslett,M., Aurrecoechea,C., Berriman,M., Brestelli,J., Brunk,B.P., Carrington,M., Depledge,D.P., Fischer,S., Gajria,B., Gao,X. *et al.* (2010) TriTrypDB: a functional genomic resource for the Trypanosomatidae. *Nucleic Acids Res.*, **38**, D457–D462.
19. Dumetz,F., Imamura,H., Sanders,M., Seblova,V., Myskova,J., Pescher,P., Vanaerschot,M., Meehan,C.J., Cuypers,B., De Muylder,G. *et al.* (2017) Modulation of Aneuploidy in Leishmania donovani during adaptation to different in vitro and in vivo environments and its impact on gene expression. *mBio*, **8**, e00599-17.
20. Farajnia,S., Alimohammadian,M.H., Reiner,N.E., Karimi,M., Ajdari,S. and Mahboudi,F. (2004) Molecular characterization of a novel amastigote stage specific Class I nuclease from Leishmania major. *Int. J. Parasitol.*, **34**, 899–908.
21. Granneman,S., Petfalski,E., Swiatkowska,A. and Tollervey,D. (2010) Cracking pre-40S ribosomal subunit structure by systematic analyses of RNA-protein cross-linking. *EMBO J.*, **29**, 2026–2036.
22. Beausoleil,S.A., Villen,J., Gerber,S.A., Rush,J. and Gygi,S.P. (2006) A probability-based approach for high-throughput protein phosphorylation analysis and site localization. *Nat. Biotechnol.*, **24**, 1285–1292.
23. Smith,C.A., Want,E.J., O'Maille,G., Abagyan,R. and Siuzdak,G. (2006) XCMS: processing mass spectrometry data for metabolite profiling using nonlinear peak alignment, matching, and identification. *Anal. Chem.*, **78**, 779–787.
24. Tautenhahn,R., Bottcher,C. and Neumann,S. (2008) Highly sensitive feature detection for high resolution LC/MS. *BMC Bioinformatics*, **9**, 504.
25. El-Gebali,S., Mistry,J., Bateman,A., Eddy,S.R., Luciani,A., Potter,S.C., Qureshi,M., Richardson,L.J., Salazar,G.A., Smart,A. *et al.* (2019) The Pfam protein families database in 2019. *Nucleic Acids Res.*, **47**, D427–D432.
26. Buchan,D.W.A. and Jones,D.T. (2019) The PSIPRED protein analysis workbench: 20 years on. *Nucleic Acids Res.*, **47**, W402–W407.
27. Jones,D.T. and Cozzetto,D. (2015) DISOPRED3: precise disordered region predictions with annotated protein-binding activity. *Bioinformatics*, **31**, 857–863.
28. Kelley,L.A., Mezulis,S., Yates,C.M., Wass,M.N. and Sternberg,M.J. (2015) The Phyre2 web portal for protein modeling, prediction and analysis. *Nat. Protoc.*, **10**, 845–858.
29. Hayman,M.L. and Read,L.K. (1999) Trypanosoma brucei RBP16 is a mitochondrial Y-box family protein with guide RNA binding activity. *J. Biol. Chem.*, **274**, 12067–12074.
30. Walrad,P.B., Capewell,P., Fenn,K. and Matthews,K.R. (2012) The post-transcriptional trans-acting regulator, TbZFP3, co-ordinates transmission-stage enriched mRNAs in Trypanosoma brucei. *Nucleic Acids Res.*, **40**, 2869–2883.
31. Schneider,C.A., Rasband,W.S. and Eliceiri,K.W. (2012) NIH Image to ImageJ: 25 years of image analysis. *Nat. Methods*, **9**, 671–675.
32. Walrad,P., Paterou,A., Acosta-Serrano,A. and Matthews,K.R. (2009) Differential trypanosome surface coat regulation by a CCCH protein that co-associates with procyclin mRNA cis-elements. *PLoS Pathog.*, **5**, e1000317.
33. Lighthall,G.K. and Giannini,S.H. (1992) The chromosomes of Leishmania. *Parasitol. Today*, **8**, 192–199.
34. Ong,S.E., Mittler,G. and Mann,M. (2004) Identifying and quantifying in vivo methylation sites by heavy methyl SILAC. *Nat. Methods*, **1**, 119–126.
35. Crooks,G.E., Hon,G., Chandonia,J.M. and Brenner,S.E. (2004) WebLogo: a sequence logo generator. *Genome Res*, **14**, 1188–1190.
36. Dupe,A., Dumas,C. and Papadopoulou,B. (2014) An Alba-domain protein contributes to the stage-regulated stability of amastin transcripts in Leishmania. *Mol. Microbiol.*, **91**, 548–561.
37. Dupe,A., Dumas,C. and Papadopoulou,B. (2015) Differential subcellular localization of Leishmania Alba-domain proteins throughout the parasite development. *PLoS One*, **10**, e0137243.
38. Goulah,C.C. and Read,L.K. (2007) Differential effects of arginine methylation on RBP16 mRNA binding, guide RNA (gRNA) binding, and gRNA-containing ribonucleoprotein complex (gRNP) formation. *J. Biol. Chem.*, **282**, 7181–7190.
39. Alves-Ferreira,E.V., Toledo,J.S., De Oliveira,A.H., Ferreira,T.R., Ruy,P.C., Pinzan,C.F., Santos,R.F., Boaventura,V., Rojo,D., Lopez-Gonzalvez,A. *et al.* (2015) Differential gene expression and infection profiles of cutaneous and mucosal leishmania braziliensis isolates from the same patient. *PLoS Negl. Trop. Dis.*, **9**, e0004018.
40. Debler,E.W., Jain,K., Warmack,R.A., Feng,Y., Clarke,S.G., Blobel,G. and Stavropoulos,P. (2016) A glutamate/aspartate switch controls product specificity in a protein arginine methyltransferase. *PNAS*, **113**, 2068–2073.
41. Feng,Y., Maity,R., Whitelegge,J.P., Hadjikyriacou,A., Li,Z., Zurita-Lopez,C., Al-Hadid,Q., Clark,A.T., Bedford,M.T., Masson,J.Y. *et al.* (2013) Mammalian protein arginine methyltransferase 7 (PRMT7) specifically targets RXR sites in lysine- and arginine-rich regions. *J. Biol. Chem.*, **288**, 37010–37025.
42. Cruz,A.K. and Freitas-Castro,F. (2019) Genome and transcriptome analyses of Leishmania spp.: opening Pandora's box. *Curr. Opin. Microbiol.*, **52**, 64–69.
43. Padmanabhan,P.K., Zghidi-Abouzid,O., Samant,M., Dumas,C., Aguiar,B.G., Estaquier,J. and Papadopoulou,B. (2016) DDX3 DEAD-box RNA helicase plays a central role in mitochondrial protein quality control in Leishmania. *Cell Death. Dis.*, **7**, e2406.
44. Fisk,J.C., Presnyak,V., Ammerman,M.L. and Read,L.K. (2009) Distinct and overlapping functions of MRP1/2 and RBP16 in mitochondrial RNA metabolism. *Mol. Cell. Biol.*, **29**, 5214–5225.
45. Rosenzweig,D., Smith,D., Myler,P.J., Olafson,R.W. and Zilberstein,D. (2008) Post-translational modification of cellular proteins during Leishmania donovani differentiation. *Proteomics*, **8**, 1843–1850.
46. Tsigankov,P., Gherardini,P.F., Helmer-Citterich,M., Spath,G.F. and Zilberstein,D. (2013) Phosphoproteomic analysis of differentiating Leishmania parasites reveals a unique stage-specific phosphorylation motif. *J. Proteome Res.*, **12**, 3405–3412.
47. Dhar,S., Vemulapalli,V., Patananan,A.N., Huang,G.L., Di Lorenzo,A., Richard,S., Comb,M.J., Guo,A., Clarke,S.G. and Bedford,M.T. (2013) Loss of the major Type I arginine methyltransferase PRMT1 causes substrate scavenging by other PRMTs. *Sci. Rep.*, **3**, 1311.
48. Kafkova,L., Tu,C., Pazzo,K.L., Smith,K.P., Debler,E.W., Paul,K.S., Qu,J. and Read,L.K. (2018) Trypanosoma brucei PRMT1 is a nucleic acid binding protein with a role in energy metabolism and the starvation stress response. *mBio*, **9**, e02430-18.

49. Lott,K., Zhu,L., Fisk,J.C., Tomasello,D.L. and Read,L.K. (2014) Functional interplay between protein arginine methyltransferases in Trypanosoma brucei. *Microbiology Open*, **3**, 595–609.
50. Zheng,S., Moehlenbrink,J., Lu,Y.C., Zalmas,L.P., Sagum,C.A., Carr,S., McGouran,J.F., Alexander,L., Fedorov,O., Munro,S. *et al.* (2013) Arginine methylation-dependent reader-writer interplay governs growth control by E2F-1. *Mol. Cell*, **52**, 37–51.
51. Kafkova,L., Debler,E.W., Fisk,J.C., Jain,K., Clarke,S.G. and Read,L.K. (2017) The major protein arginine methyltransferase in trypanosoma brucei functions as an Enzyme-Prozyme complex. *J. Biol. Chem.*, **292**, 2089–2100.
52. Lee,Y.H. and Stallcup,M.R. (2009) Minireview: protein arginine methylation of nonhistone proteins in transcriptional regulation. *Mol. Endocrinol.*, **23**, 425–433.
53. Gao,G., Dhar,S. and Bedford,M.T. (2017) PRMT5 regulates IRES-dependent translation via methylation of hnRNP A1. *Nucleic Acids Res.*, **45**, 4359–4369.
54. Wall,M.L. and Lewis,S.M. (2017) Methylarginines within the RGG-Motif region of hnRNP A1 affect its IRES Trans-Acting factor activity and are required for hnRNP A1 stress granule localization and formation. *J. Mol. Biol.*, **429**, 295–307.
55. Yu,M.C. (2011) The role of protein arginine methylation in mRNP dynamics. *Mol. Biol. Int.*, **2011**, 163827.
56. Cui,W., Yoneda,R., Ueda,N. and Kurokawa,R. (2018) Arginine methylation of translocated in liposarcoma (TLS) inhibits its binding to long noncoding RNA, abrogating TLS-mediated repression of CBP/p300 activity. *J. Biol. Chem.*, **293**, 10937–10948.
57. Lott,K., Mukhopadhyay,S., Li,J., Wang,J., Yao,J., Sun,Y., Qu,J. and Read,L.K. (2015) Arginine methylation of DRBD18 differentially impacts its opposing effects on the trypanosome transcriptome. *Nucleic Acids Res.*, **43**, 5501–5523.
58. de Paiva,R.M., Grazielle-Silva,V., Cardoso,M.S., Nakagaki,B.N., Mendonca-Neto,R.P., Canavaci,A.M., Souza Melo,N., Martinelli,P.M., Fernandes,A.P., daRocha,W.D. *et al.* (2015) Amastin knockdown in Leishmania braziliensis affects Parasite-Macrophage interaction and results in impaired viability of intracellular amastigotes. *PLoS Pathog.*, **11**, e1005296.
59. Paterou,A., Walrad,P., Craddy,P., Fenn,K. and Matthews,K. (2006) Identification and stage-specific association with the translational apparatus of TbZFP3, a CCCH protein that promotes trypanosome life-cycle development. *J. Biol. Chem.*, **281**, 39002–39013.
60. da Costa,K.S., Galucio,J.M.P., Leonardo,E.S., Cardoso,G., Leal,E., Conde,G. and Lameira,J. (2017) Structural and evolutionary analysis of Leishmania Alba proteins. *Mol. Biochem. Parasitol.*, **217**, 23–31.
61. Miller,M.M., Halbig,K., Cruz-Reyes,J. and Read,L.K. (2006) RBP16 stimulates trypanosome RNA editing in vitro at an early step in the editing reaction. *RNA*, **12**, 1292–1303.
62. Besteiro,S., Williams,R.A., Coombs,G.H. and Mottram,J.C. (2007) Protein turnover and differentiation in Leishmania. *Int. J. Parasitol.*, **37**, 1063–1075.
63. Hu,D., Gur,M., Zhou,Z., Gamper,A., Hung,M.C., Fujita,N., Lan,L., Bahar,I. and Wan,Y. (2015) Interplay between arginine methylation and ubiquitylation regulates KLF4-mediated genome stability and carcinogenesis. *Nat. Commun.*, **6**, 8419.
64. Tikhanovich,I., Kuravi,S., Artigues,A., Villar,M.T., Dorko,K., Nawabi,A., Roberts,B. and Weinman,S.A. (2015) Dynamic arginine methylation of tumor necrosis factor (TNF) receptor-associated factor 6 regulates toll-like receptor signaling. *J. Biol. Chem.*, **290**, 22236–22249.
65. Kruger,T., Hofweber,M. and Kramer,S. (2013) SCD6 induces ribonucleoprotein granule formation in trypanosomes in a translation-independent manner, regulated by its Lsm and RGG domains. *Mol. Biol. Cell*, **24**, 2098–2111.
66. Fritz,M., Vanselow,J., Sauer,N., Lamer,S., Goos,C., Siegel,T.N., Subota,I., Schlosser,A., Carrington,M. and Kramer,S. (2015) Novel insights into RNP granules by employing the trypanosome's microtubule skeleton as a molecular sieve. *Nucleic Acids Res.*, **43**, 8013–8032.